AEDC-TR-67-149

cy 3

FLOW FIELD OF A SONIC JET EXHAUSTING COUNTER TO A LOW DENSITY SUPERSONIC AIRSTREAM

Robert A. Cassanova

ARO, Inc.

October 1967

AEROSPACE ENVIRONMENTAL FACILITY
ARNOLD ENGINEERING DEVELOPMENT CENTER
AIR FORCE SYSTEMS COMMAND
ARNOLD AIR FORCE STATION, TENNESSEE

NOTICES

When U. S. Government drawings specifications, or other data are used for any purpose other than a definitely related Government procurement operation, the Government thereby incurs no responsibility nor any obligation whatsoever, and the fact that the Government may have formulated, furnished, or in any way supplied the said drawings, specifications, or other data, is not to be regarded by implication or otherwise, or in any manner licensing the holder or any other person or corporation, or conveying any rights or permission to manufacture, use, or sell any patented invention that may in any way be related thereto.

Qualified users may obtain copies of this report from the Defense Documentation Center.

References to named commercial products in this report are not to be considered in any sense as an endorsement of the product by the United States Air Force or the Government.

FLOW FIELD OF A SONIC JET EXHAUSTING COUNTER TO A LOW DENSITY SUPERSONIC AIRSTREAM

Robert A. Cassanova
ARO, Inc.

FOREWORD

The work reported herein was sponsored by the Air Force Cambridge Research Laboratory (CRUI), Air Force Systems Command (AFSC), under Program Element 62405424, Project 7635.

The results of tests presented were obtained by ARO, Inc. (a subsidiary of Sverdrup & Parcel and Associates, Inc.), contract operator of Arnold Engineering Development Center (AEDC), AFSC, Arnold Air Force Station, Tennessee, under Contract AF40(600)-1200. The tests were conducted under ARO Project No. SB0609 in the Aerospace Research Chamber (8V), and the manuscript was submitted for publication on May 23, 1967.

The work reported herein has also been used as a thesis for partial fulfillment of the requirements for the degree of master of science from the University of Tennessee. The author wishes to express his appreciation to Dr. Ying-Chu Lin Wu, professor of aerospace engineering at the University of Tennessee Space Institute, for her direction throughout the course of this investigation.

This technical report has been reviewed and is approved.

Paul L. Landry
Major, USAF
AF Representative, AEF
Directorate of Test

Leonard T. Glaser
Colonel, USAF
Director of Test

ABSTRACT

The flow field of a sonic jet exhausting counter to a supersonic airstream has been investigated theoretically and experimentally. The total shock-layer thickness was calculated using a blunt-body-type analysis and the known properties of a free-jet expansion from a sonic orifice. The total shock-layer thickness and position of the outer shock relative to the orifice are shown to be a function of free-stream Mach number, jet reservoir pressure, free-stream pitot pressure, and orifice size. The predicted inner shock position is compared with previously published experimental data, and the predicted outer shock position is compared with data obtained in a low density wind tunnel. Results in the transitional flow regime indicate that the outer shock to orifice position distance is greater than the predicted value.

CONTENTS

ILLUSTRATIONS

TABLES

NOMENCLATURE

C_p	Coefficient of pressure
D	Diameter of orifice
M	Mach number
m	Molecular weight
P	Pressure
R	Distance from orifice exit
$\hat{R}$	Gas constant
Re	Reynolds number
U	Flow velocity
u	Velocity parallel to contact surface
v	Velocity normal to contact surface
X	Distance along centerline from orifice exit
x	Distance parallel to contact surface
y	Distance normal to contact surface
γ	Ratio of specific heats
Δ	Shock detachment distance
ϵ	Density ratio across shock
λ	Mean free path
μ	Viscosity
Φ	Flow angle measured from orifice centerline

SUBSCRIPTS

1	Static conditions in front of shock
2	Static conditions behind a normal shock

c	Contact surface
e	Outer shock
equiv	Equivalent
exp	Experimental
j	Jet
max	Maximum
o	Total conditions
theo	Theoretical
Δ	Shock detachment distance
∞	Free stream

SUPERSCRIPTS

$'$	Stagnation conditions behind normal shock
*	Sonic conditions

SECTION I
INTRODUCTION

The flow pattern of a jet exhausting counter to a supersonic free stream has been investigated by several authors from the standpoint of application to thrust vector control and thermal protection of the re-entry vehicle (Refs. 1, 2, and 3). More recently the case of a sonic jet exhausting from the nose of a sounding rocket at high altitudes has become important. As part of the AFCRL upper atmosphere research program, nitric oxide (NO) was released from the nose of sounding rockets in the upper atmosphere (90- to 140-km altitude) at night to determine the atomic oxygen (O_2) concentration. A series of tests simulating the rocket flights was performed at AEDC to determine the effective rate constant (K) for the reaction, $NO + 0 \overset{K}{\rightleftharpoons} NO_2 + h\nu$. Results of these tests are reported in Refs. 4, 5, and 6. This report presents an inviscid analysis of the flow field of a sonic jet exhausting counter to a supersonic free stream and discusses the effects of flow rarefaction on the flow field. Previous experimental results (Refs. 1, 2, and 3) are compared with the present theory, and data obtained from a low density wind tunnel are presented. The analysis neglects chemical reactions in the shock layer.

SECTION II
FREE-JET FLOW FIELD

The flow field of the sonic jet expanding into a vacuum has been investigated by Ashkenas and Sherman (Ref. 7), who obtained fitting formulas from a method of characteristics solution of the flow. From experimental pitot probe data, Ashkenas and Sherman obtained the following formula along the centerline for $2 < X/D < 90$:

$$\frac{P'_{oj}}{P_{oj}} = 0.640 \left(\frac{X}{D}\right)^{-2.07} \quad \text{for } \gamma = \frac{7}{5} \tag{1}$$

X = distance along centerline from orifice exit,

D = diameter of orifice,

P'_{oj} = pitot pressure behind a normal shock, and

P_{oj} = jet reservoir pressure.

Ashkenas and Sherman also compared the results obtained by using a sonic nozzle and a thin plate orifice and found that for the round orifice,

the effects of entrance geometry on the flow field were negligible for $Re_{D^*} > 600$, where Re_{D^*} equals Reynolds number based on the orifice diameter. However, viscous effects began reducing the effective orifice diameter in the nozzle orifice at $Re_{D^*} < 600$. This point will be discussed again later with the present experimental results in Section 6.2.

SECTION III
FLOW FIELD CONFIGURATION

A detailed sketch of the inviscid flow field is shown in Fig. 1 and serves to define symbols.

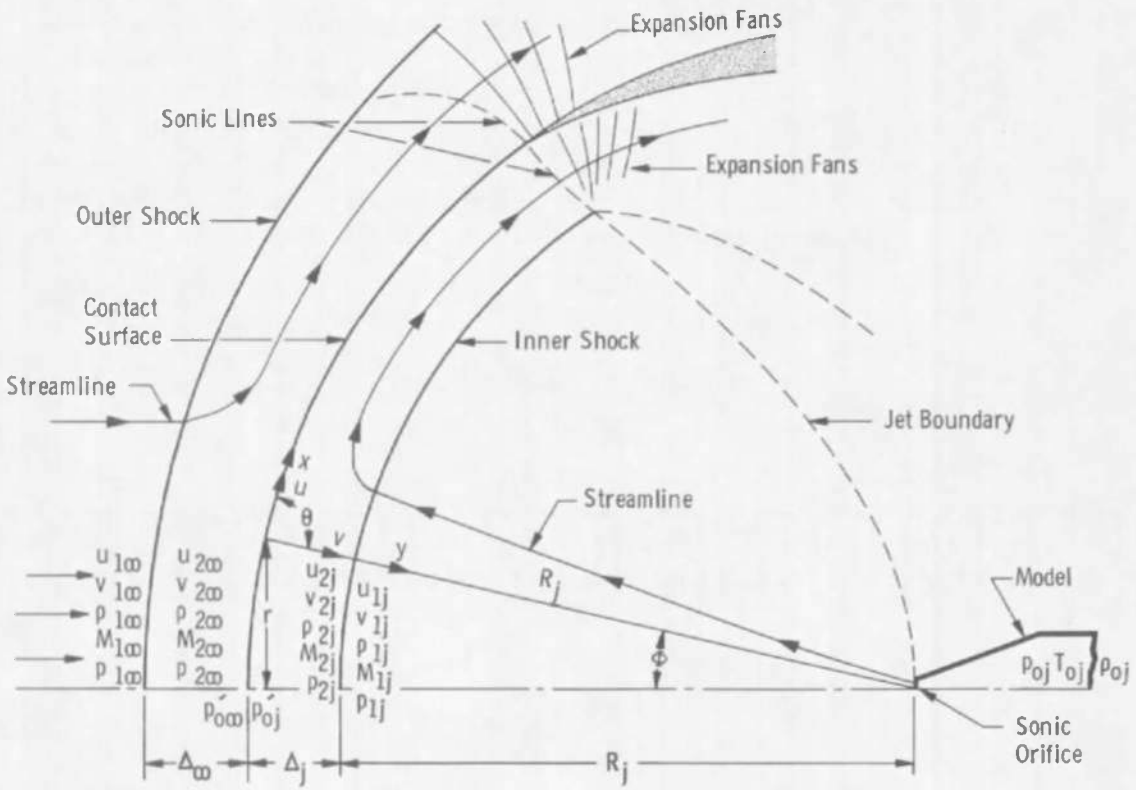

Fig. 1 Flow Field and Nomenclature, Sonic Jet Exhausting Counter to a Supersonic Airstream

3.1 GENERAL STRUCTURE

The general configuration has been investigated (Refs. 1 and 2) and consists of an outer shock through which the free stream is decelerated, an inner shock through which the jet flow is decelerated, and a contact

surface where the two flows meet and the pressure of the two flows at the contact surface must equilibrate. The shock pattern is in the form of an approximate spherical shell with the flow between the two shocks expanding to the ambient conditions at a "shoulder point" located where the jet boundary meets the inner shock.

3.2 CONTACT SURFACE SHAPE

It can be shown that the contact surface is approximately spherical by comparing the pressure distribution on the free-stream side of the contact surface with the pressure on the jet side. The pressure distribution on the free-stream side is obtained from a modified Newtonian analysis with the contact surface assumed a solid sphere, or

$$\frac{P}{P'_{2\infty}} = \cos^2 \Phi + \frac{P_{1\infty}}{P'_{2\infty}} \sin^2 \Phi \tag{2}$$

where

P = pressure at contact surface,

$P'_{2\infty}$ = pressure at stagnation point on contact surface, and

$P_{1\infty}$ = free-stream static pressure

which is plotted in Fig. 2. The pressure distribution on the jet side is obtained by using the formula derived by Sherman (Ref. 8) for the density ratio as a function of Φ,

$$\frac{\rho_{1j}}{\rho_{oj}} = \frac{0.357}{R^2} \cos^2 (0.945\Phi) \text{ for } \gamma = \frac{7}{5} \tag{3}$$

ρ_{1j} = static density in the free jet,

ρ_{oj} = jet reservoir density, and

R = distance from orifice exit

from which the free-jet Mach number and pressure ratio across the inner shock (assumed normal) can be calculated from isentropic relations. The calculated distribution is compared with the modified Newtonian result in Fig. 2. The pressure distributions agree very closely, confirming the approximate spherical nature of the contact surface.

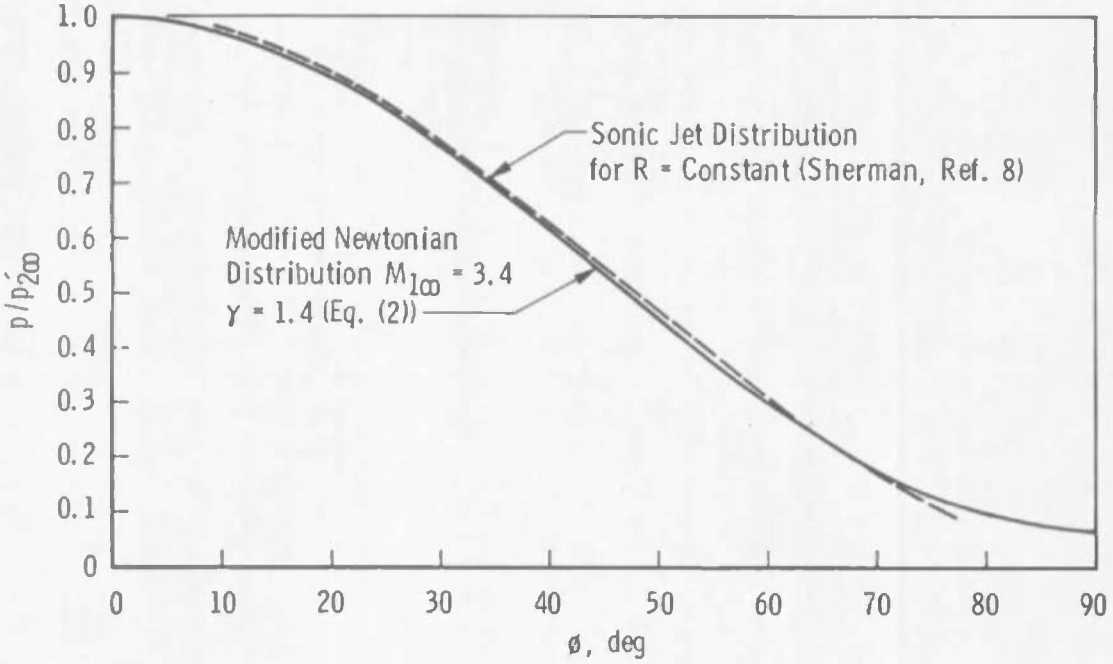

Fig. 2 Pressure Distribution on Contact Surface

3.3 INNER SHOCK LOCATION

Previous experimental data for continuum air for the inner shock location on the jet axis are summarized in Fig. 3 along with Charwat's (Ref. 3) theory for the inner shock location. The experimental data (Refs. 2 and 3) were obtained from schlieren photographs at M_∞ = 2.9 to 7.1.

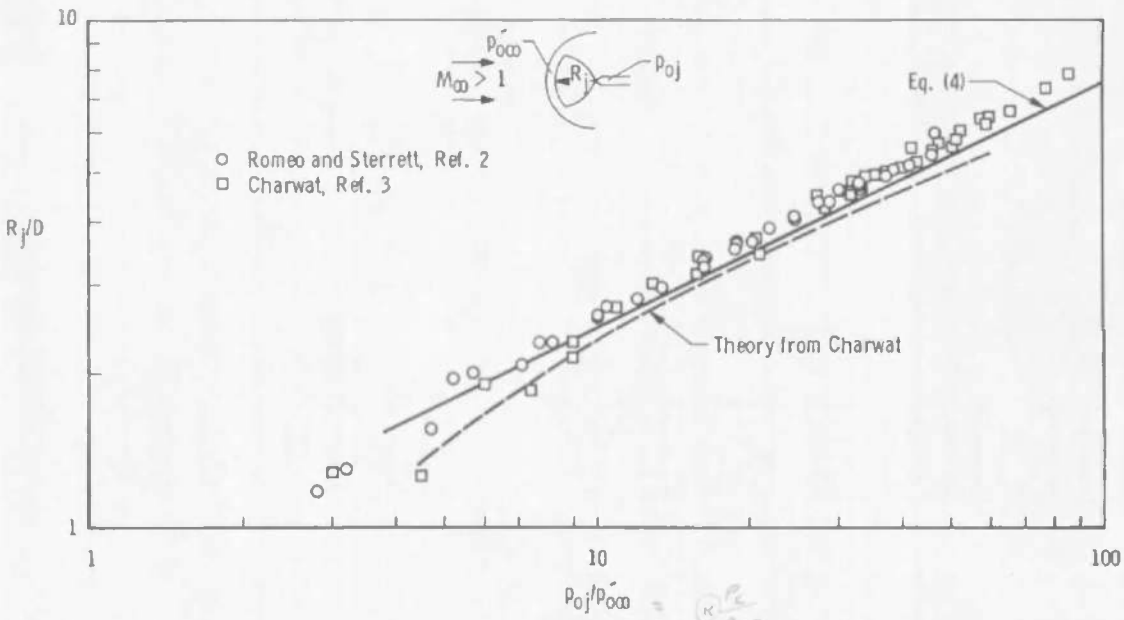

Fig. 3 Inner Shock Location

The inner shock location can also be found from Eq. (1) by assuming that the free-jet pitot pressure behind a normal shock equates with the free-stream pitot pressure along the jet centerline; i. e.,

$$P'_{oj} = P'_{o\infty}$$

$$\frac{X}{D} = \frac{R_j}{D} = 0.806 \left(\frac{P_{oj}}{P'_{o\infty}}\right)^{0.483} \tag{4}$$

which is plotted in Fig. 3. Equation (4) does give somewhat better agreement with the experimental shock locations and will be used in further derivations.

SECTION IV
SHOCK-LAYER THICKNESS

4.1 INVISCID SOLUTION FOR THE FLOW FIELD BETWEEN THE CONTACT SURFACE AND THE INNER SHOCK

The flow field between the inner shock and the contact surface is analogous to a blunt-body flow field where the shock is detached from the surface. Upon analysis of the known parameters, it is found that a hypersonic blunt-body analysis, similar to Li and Geiger's constant density solution (Ref. 9) can be adapted to the present flow field to solve for the shock-layer thickness at the stagnation point. A correlation between free-stream conditions, jet-stream conditions, jet total conditions, and shock detachment distance, Δ_j, can be made. Previous experimental data on blunt bodies in hypersonic flow (Ref. 9) have shown Li and Geiger's solution to be accurate for hypersonic Mach numbers, which is the case for the jet flow fields considered here.

The following derivation and discussion review, in part, Li and Geiger's derivation and apply boundary conditions and assumptions appropriate for the present flow field. Symbols are defined in Fig. 1.

The basic equations of motion governing the axisymmetric flow of an inviscid fluid are:

$$\left[\frac{1}{(1 + Ky)}\right] u \frac{\partial u}{\partial x} + v \frac{\partial u}{\partial y} + \left[\frac{K}{(1 + Ky)}\right] uv$$

$$+ \frac{1}{(1 + Ky)} \frac{1}{\rho} \frac{\partial P}{\partial x} = 0 \tag{5}$$

$$\left[\frac{1}{(1+Ky)}\right] u \frac{\partial v}{\partial x} + v \frac{\partial v}{\partial y} - \left[\frac{K}{(1+Ky)}\right] u^2$$

$$+ \frac{1}{\rho} \frac{\partial P}{\partial y} = 0 \tag{6}$$

$$\left[\frac{1}{(1+Ky)}\right] \frac{\partial}{\partial x} (\rho u) + \frac{\partial}{\partial y} (\rho v) + \left[\frac{K}{(1+Ky)}\right] \rho v$$

$$+ \frac{1}{r} \left\{ \left[\frac{\rho u}{(1+Ky)}\right] \frac{\partial r}{\partial x} + \rho v \frac{\partial r}{\partial y} \right\} = 0 \tag{7}$$

where x and y are distances measured along, and normal to, the contact surface, K is the curvature of the contact surface, or $K = 1/R_c$.

Certain simplifications can be applied to the governing equations:

1. Since Δ_j is small in comparison to R_c and $Ky = 0(\Delta_j/R_c)$, then $Ky \ll 1$.
2. Since the velocities in the shock layer at the stagnation point (u, v) are small, then terms Kuv and Ku^2 can be neglected.
3. In the vicinity of the stagnation point, $r \approx x$. Therefore, for small r, r can be replaced by x.
4. As $M_{1j} \longrightarrow \infty$, $M_{2j} \longrightarrow (\gamma - 1)/2\gamma$. Therefore, the flow field near the stagnation point can be regarded as essentially incompressible, or $\rho \approx \rho_{2j} = \rho_{1j}/\epsilon$.

Applying these simplifications to Eqs. (5), (6), and (7), the governing equations become:

$$u \frac{\partial u}{\partial x} + v \frac{\partial u}{\partial y} = - \frac{\epsilon}{\rho_{1j}} \frac{\partial P}{\partial x} \tag{8}$$

$$u \frac{\partial v}{\partial x} + v \frac{\partial v}{\partial y} = - \frac{\epsilon}{\rho_{1j}} \frac{\partial P}{\partial x} \tag{9}$$

$$\frac{\partial (ux)}{\partial x} + \frac{\partial (vx)}{\partial y} = 0 \tag{10}$$

The appropriate boundary conditions are:

1. Stagnation conditions on the contact surface, $y = 0$, $x = 0$, then $u = v = 0$.

2. Condition of tangency along the contact surface is $y = 0$, $v = 0$.
3. Conditions along the inner shock are $y = \Delta_j$, $u = 0$, $v_{2j} = (\rho_{1j}/\rho_{2j})v_{1j}$.
4. Conditions along the contact surface were defined in the previous section by matching the flow in the inner shock layer with the flow in the outer shock layer. It was shown that the pressure distribution was equivalent to the modified Newtonian distribution,

$$C_p = C_{p_o} \cos^2 \Phi$$

or

$$\frac{P}{P'_{o_j}} = \cos^2 \Phi + \frac{P_{1_j}}{P'_{o_j}} \sin^2 \Phi \tag{11}$$

The incompressible Bernoulli equation in the stagnation region is:

$$P'_{o_j} = P + \frac{1}{2} \rho'_{o_j} u^2 \tag{12}$$

or

$$u = \sqrt{\frac{2P'_{o_j}}{\rho'_{o_j}} \left(1 - \frac{P}{P'_{o_j}}\right)} \tag{13}$$

Substituting Eq. (11) into Eq. (13),

$$u = \sin \Phi \sqrt{\frac{2P'_{o_j}}{\rho'_{o_j}} \left(1 - \frac{P_{1_j}}{P'_{o_j}}\right)} \tag{14}$$

If Φ is small, then $\sin \Phi \approx \Phi$ and $x \approx R_j \Phi$. Therefore,

$$u = \frac{x}{R_j} \sqrt{\frac{2P'_{o_j}}{\rho'_{o_j}} \left(1 - \frac{P_{1_j}}{P'_{o_j}}\right)} \tag{15}$$

4.2 SOLUTION FOR THE INNER SHOCK DETACHMENT DISTANCE

The P is first eliminated from Eqs. (8) and (9) by differentiating Eq. (8) with $\partial/\partial y$ and Eq. (9) with $\partial/\partial x$, or

$$\frac{\partial u}{\partial y} \frac{\partial u}{\partial x} + u \frac{\partial^2 u}{\partial x \partial y} + \frac{\partial v}{\partial y} \frac{\partial u}{\partial y} + v \frac{\partial^2 u}{\partial y^2} =$$

$$- \frac{\epsilon}{\rho_{1_j}} \frac{\partial^2 P}{\partial x \partial y} \tag{16}$$

$$\frac{\partial u}{\partial x}\frac{\partial v}{\partial x} + u\frac{\partial^2 v}{\partial x^2} + \frac{\partial v}{\partial x}\frac{\partial v}{\partial y} + v\frac{\partial^2 v}{\partial x \partial y} =$$

$$-\frac{\epsilon}{\rho_{1j}}\frac{\partial^2 P}{\partial x \partial y} \tag{17}$$

By subtracting, one obtains:

$$\frac{\partial u}{\partial y}\frac{\partial u}{\partial x} + u\frac{\partial^2 u}{\partial x \partial y} + \frac{\partial v}{\partial y}\frac{\partial u}{\partial y} + v\frac{\partial^2 u}{\partial y^2} - \frac{\partial u}{\partial x}\frac{\partial v}{\partial x}$$

$$- u\frac{\partial^2 v}{\partial x^2} - \frac{\partial v}{\partial x}\frac{\partial v}{\partial y} - v\frac{\partial^2 v}{\partial x \partial y} = 0 \tag{18}$$

Combining terms in Eq. (12):

$$u\left[\frac{\partial^2 u}{\partial x \partial y} - \frac{\partial^2 v}{\partial x^2}\right] + v\left[\frac{\partial^2 u}{\partial y^2} - \frac{\partial^2 v}{\partial x \partial y}\right]$$

$$+ \frac{\partial v}{\partial y}\left[\frac{\partial u}{\partial y} - \frac{\partial v}{\partial x}\right] + \frac{\partial u}{\partial x}\left[\frac{\partial u}{\partial y} - \frac{\partial v}{\partial x}\right] = 0 \tag{19}$$

The form of u and v must be chosen, and the following argument is presented by Li and Geiger (Ref. 9). For small x, u(x, y) may be expressed as an ascending series of the form,

$$u(x,y) = a_0 + a_1 x + a_2 x^2 + \ldots \tag{20}$$

where the a's are functions of y. The symmetry of the problem permits only terms in odd powers of x, and for small x's third and higher order terms are unimportant. Therefore, it can be assumed that

$$u = x\,f'(y) \tag{21}$$

where $f' = \partial f/\partial y$, or a linear variation of u with respect to x near the stagnation point. Substituting Eq. (21) into the continuity Eq. (10), the form of v is:

$$v = -2\,f(y) \tag{22}$$

Equations (19), (21), and (22) are now combined in the following manner:

$$xf'(f'' - 0) - 2f(xf''' - 0) - 2f'(xf'' - 0) + f'(xf'' - 0) = 0 \tag{23}$$

where $f'' = \partial^2 f/\partial y^2$ and $f''' = \partial^3 f/\partial y^3$, or

$$-2xff''' = 0 \tag{24}$$

and since $f \neq 0$, then

$$f''' = 0 \tag{25}$$

Equation (25) is a simple differential equation which can be solved to yield:

$$f(y) = C_o + C_1 y + C_2 y^2 = -\frac{v}{2} \tag{26}$$

where the constants of integration must be determined from the boundary conditions.

The condition of tangency ($y = 0$, $v = 0$) yields $C_o = 0$.

The constants C_1 and C_2 are determined from the conditions at the inner shock.

As $x \longrightarrow 0$

$$y = \Delta_j$$

or

$$f(\Delta_j) = C_1\Delta_j + C_2\Delta^2_j$$

but

$$f(\Delta_j) = +\frac{v_{2j}}{2}$$

and, since

$$v = -v_{2j} = -\frac{\rho_{1j}}{\rho_{2j}} v_{1j} = -\epsilon v_{1j}$$

or

$$C_1\Delta_j + C_2\Delta^2_j = +\frac{\epsilon}{2} v_{1j} \tag{27}$$

From Eq. (21),

$$f'(y) = C_1 + 2C_2 y = \frac{u}{x}$$

and, as $x \longrightarrow 0$, $y \longrightarrow \Delta j$; therefore,

$$C_1 + 2C_2\Delta_j = \lim_{x \to 0} \left(\frac{u}{x}\right) \tag{28}$$

but from Eq. (15),

$$\lim_{x \to 0} \left(\frac{u}{x}\right) = \frac{1}{R_j}\sqrt{\frac{2P'_{oj}}{\rho'_{oj}}\left(1 - \frac{P_{1j}}{P'_{oj}}\right)} \tag{29}$$

Substituting Eq. (28) into Eq. (29):

$$C_1 + 2C_2\Delta_j = \frac{1}{R_j}\sqrt{\frac{2P'_{oj}}{\rho'_{oj}}\left(1 - \frac{P_{1j}}{P'_{oj}}\right)} \tag{30}$$

Equations (27) and (30) can now be solved simultaneously for C_1 and C_2 in terms of Δ_j, R_j, P'_{oj}, ρ'_{oj}, P, ϵ, and v_{1j}. Or,

$$C_1 = + \frac{\epsilon v_{1j}}{\Delta_j} - \frac{1}{R_j}\sqrt{\frac{2P'_{oj}}{\rho'_{oj}}\left(1 - \frac{P_{1j}}{P'_{oj}}\right)} \tag{31}$$

$$C_2 = - \frac{\epsilon v_{1j}}{2\Delta_j^2} + \frac{1}{\Delta_j R_j}\sqrt{\frac{2P'_{oj}}{\rho'_{oj}}\left(1 - \frac{P_{1j}}{P'_{oj}}\right)} \tag{32}$$

To solve for Δ_j, $\partial P/\partial x$ is found from Eq. (11) and substituted into Eq. (8) along with Eqs. (21) and (22). Then C_1 can be found in terms of R_j, P'_{oj}, ρ'_{oj}, and P_{1j}. From Eq. (11),

$$\frac{\partial P}{\partial x} = -2P'_{oj}\left(1 - \frac{P_{1j}}{P'_{oj}}\right)\sin\Phi\cos\Phi\frac{\partial\Phi}{\partial x} \tag{33}$$

and

$$xf''^2 - 2xff''' = \frac{2\epsilon}{\rho_{1j}}\left[P'_{oj}\left(1 - \frac{P_{1j}}{P'_{oj}}\right)\sin\Phi\cos\Phi\frac{\partial\Phi}{\partial x}\right]$$

or

$$f''^2 - 2ff''' = \left[\frac{2P'_{oj}}{\rho'_{oj}}\left(1 - \frac{P_{1j}}{P'_{oj}}\right)\frac{\sin\Phi}{x}\cos\Phi\frac{\partial\Phi}{\partial x}\right] \tag{34}$$

as $x \to 0$, $(\sin\Phi)/x \to 1/R_j$, $\cos\Phi \to 1$, and $(\partial\Phi/\partial x) \to 1/R_j$. Therefore,

$$f''^2 - 2ff''' = \left[\frac{2P'_{oj}}{\rho'_{oj}}\left(1 - \frac{P_{1j}}{P'_{oj}}\right)\right]\frac{1}{R_j^2} \tag{35}$$

Substituting Eqs. (26) and (32) into (35) and solving for C_1:

$$C_1 = \pm\frac{1}{R_j}\sqrt{\frac{2P'_{oj}}{\rho'_{oj}}\left(1 - \frac{P_{1j}}{P'_{oj}}\right)} \tag{36}$$

Substituting Eq. (36) into Eq. (31) and choosing the (+) sign in Eq. (36),

$$\Delta_j = \frac{R_j \epsilon v_{ij}}{\sqrt{\frac{2P'_{oj}}{\rho'_{oj}}}\left[2\left(1 - \frac{P_{ij}}{P'_{oj}}\right)^{1/2}\right]} \tag{37}$$

but

$$v_{ij} = \left(\frac{v_{ij}}{v_{jmax}}\right) v_{jmax} = \left(\frac{v_{ij}}{v_{jmax}}\right)\sqrt{\frac{2\gamma}{\gamma - 1}\left(\frac{T_o \hat{R}}{m}\right)}$$

and since

$$\frac{v_{ij}}{v_{jmax}} \approx 1 \text{ for } M_{ij} \gg 1$$

Therefore,

$$v_{ij} \approx \sqrt{\frac{2\gamma}{\gamma - 1}\left(\frac{T_o \hat{R}}{m}\right)}$$

and also,

$$\rho'_{oj} = \frac{mP'_{oj}}{\hat{R}T'_{oj}} = \frac{mP'_{oj}}{RT_{oj}}, \text{ since } T_{oj} = T'_{oj}$$

and since

$$1 - \left(\frac{P_{ij}}{P'_{oj}}\right) \approx 1, \text{ and } \epsilon = \frac{1}{6} \ (\gamma = 1.4) \text{ for } M_{ij} \gg 1$$

Then,

$$\Delta_j = 0.156R_j \text{ for } \gamma = 1.4 \tag{38}$$

Equation (4) relates R_j to the ratio of jet reservoir pressure to free-stream pitot pressure. Therefore, substituting Eq. (4) into Eq. (38) yields:

$$\Delta_j = 0.1257D\left(\frac{P_{oj}}{P'_{o\infty}}\right)^{0.483} \tag{39}$$

or

$$R_c = R_j - \Delta_j = 0.932D\left(\frac{P_{oj}}{P'_{o\infty}}\right)^{0.483} \tag{40}$$

Equation (40) shows that the contact surface location is related to the orifice size, D, and to the ratio of the jet reservoir pressure/free-stream pitot pressure ($P_{0j}/P'_{0\infty}$). Note that Eq. (40) produces accurate predictions for hypersonic free-jet Mach numbers, i.e., $M_{1j} > 5$. From Ashkenas and Sherman (Ref. 7) $M_{1j} = 5$ occurs at approximately $x/D = 3.1$ or from Eq. (1), $P_{0j}/P'_{0\infty} = 16.3$ which should be considered the lower pressure ratio limit of applicability of Eq. (40).

4.3 DETACHMENT DISTANCE OF OUTER SHOCK FROM CONTACT SURFACE

The distance from the contact surface position to the outer shock is determined by assuming the contact surface to be an equivalent spherical body and calculating an equivalent shock detachment distance using available numerically calculated results, Eq. (10). For hypersonic flow the constant density assumption for the shock layer is an accurate approximation since the Mach numbers in the shock layer are low (from $\rho_1/\rho_2 \longrightarrow$ small), and the density is essentially constant from the shock to the body. However, for supersonic flow the density ratio is no longer small, and velocities in the shock layer are relatively high, producing large density gradients between the shock and body (contact surface). Hence, the numerical calculations of Van Dyke (Ref. 10), which show good agreement with experiment in the low Mach number range, are used to determine Δ_∞ (Fig. 4).

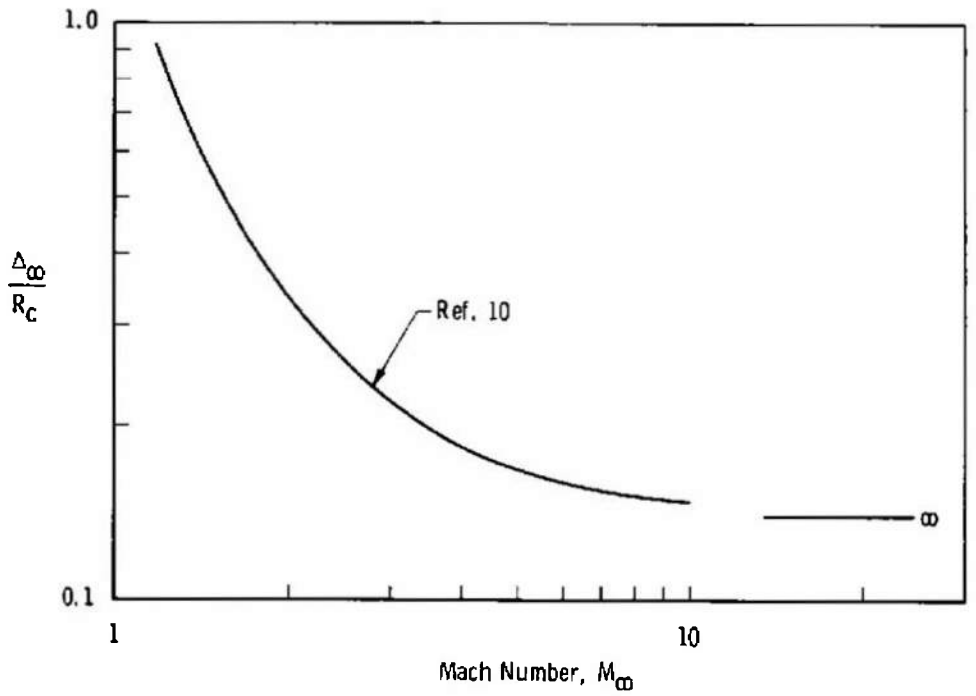

Fig. 4 Outer Shock Detachment Distance from Contact Surface

Therefore, the distance from the orifice exit to the outer shock is:

$$R_e = R_c + \frac{\Delta_\infty}{R_c} R_c \tag{41}$$

$$= 0.932D \left(\frac{P_{oj}}{P'_{o\infty}}\right)^{0.483} \left[1 + \frac{\Delta_\infty}{R_c}\right] \tag{42}$$

where Δ_∞/R_C is found for M_∞ from Fig. 4.

SECTION V
EXPERIMENTS

5.1 TEST CHAMBER

The tests were conducted in the Aerospace Research Chamber (8V), (ARC 8V) at AEDC. The pumping system for the ARC 8V consists of a 6-in. oil diffusion pump backed by a 140-cfm mechanical pump which is used for rough pumping of the chamber. During continuous runs, the gas flow is cryogenically pumped on liquid nitrogen (LN_2) (77°K) and gaseous helium (GHe) (20°K) cryosurfaces totaling 1140 ft^2. Run times from 10 to 20 min could be made at normal operating mass flow rates. A nominal Mach number 3 open test section nozzle was used to produce the supersonic free stream against which the sonic jet exhausted (Fig. 5).

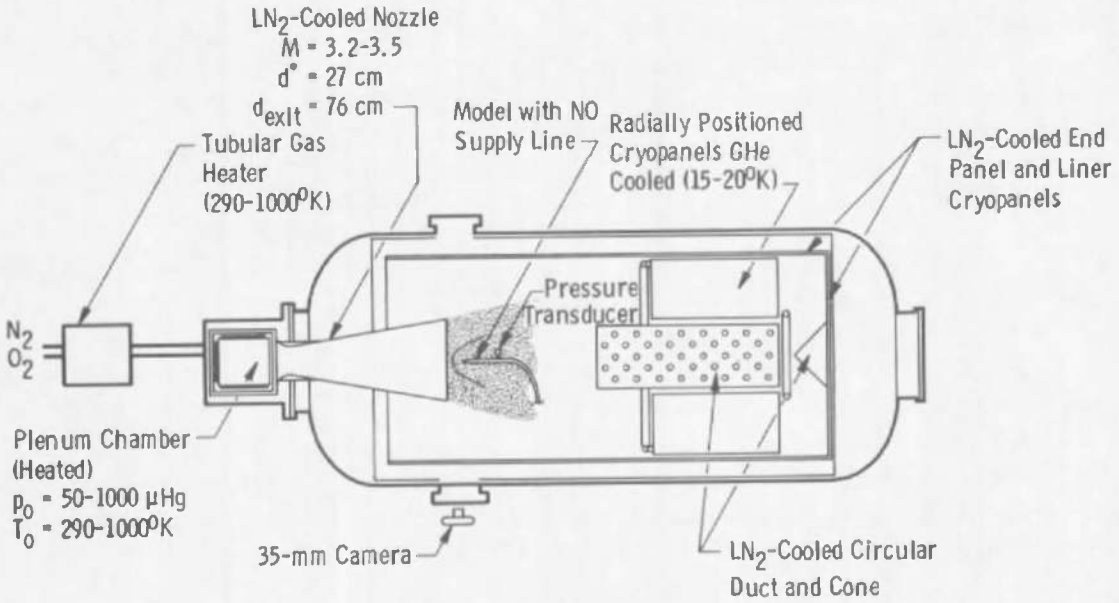

Fig. 5 Top View Schematic of Low Density Wind Tunnel (ARC 8V)

A mixture of approximately 80 percent N_2 - 20 percent O_2 was used for the supersonic nozzle flow. Three models were tested. The models were designed so that an adequate (5- to 10-cm) size outer shock radius would be produced over the range of pressure ratios, $P_{oj}/P'_{o\infty}$ = 10 to 10^4. Test conditions are listed in Table I. Nitric oxide was used in the models since this gas was being used in a simultaneous investigation of the chemiluminescent reaction of NO + O_2 reported in Ref. 9.

TABLE I
WIND TUNNEL CONDITIONS

$P_{o\infty}$, μ Hg	$P'_{o\infty}$, μ Hg	$T_{o\infty}$, °K	M_∞	λ_∞, cm	Re/ℓ, cm^{-1}	Core Diameter, cm
98.6	25.5	290	3.27	0.54	8.9	27
198.5	47.0	290	3.38	0.29	17.2	40
298.5	67.0	290	3.44	0.202	25.0	45
379.0	81.5	290	3.49	0.165	31.5	50
104.0	29.0	700	3.19	1.60	2.9	20
301.0	70.0	700	3.40	0.64	8.0	30

5.2 NOZZLE CALIBRATION

The nozzle was calibrated with a pitot probe over the range of reservoir pressures ($P_{o\infty}$) and total temperature ($T_{o\infty}$) used for the tests. The actual Mach number and other free-stream parameters are listed in Table I. The Mach number variation is caused by the change in nozzle boundary-layer thickness as the nozzle flow density changes with reservoir conditions. The usable test core diameter varied from 20 to 50 cm for the test conditions listed.

5.3 MODELS

Three models were tested (Fig. 6). The orifice diameters were 0.05, 0.15, and 0.5 in., respectively. Reservoir pressure (P_{oj}) in the models was measured with strain-gage transducers on the two smaller models (D = 0.05, 0.15 in., P_{oj} = 5 to 220 mm Hg) and with a capacitance transducer on the largest model (D = 0.5 in., P_{oj} = 0.5 to 2.2 mm Hg).

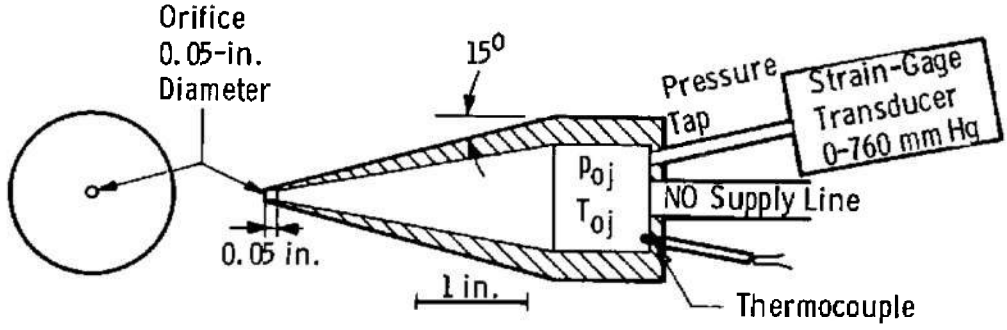

a. Model 1

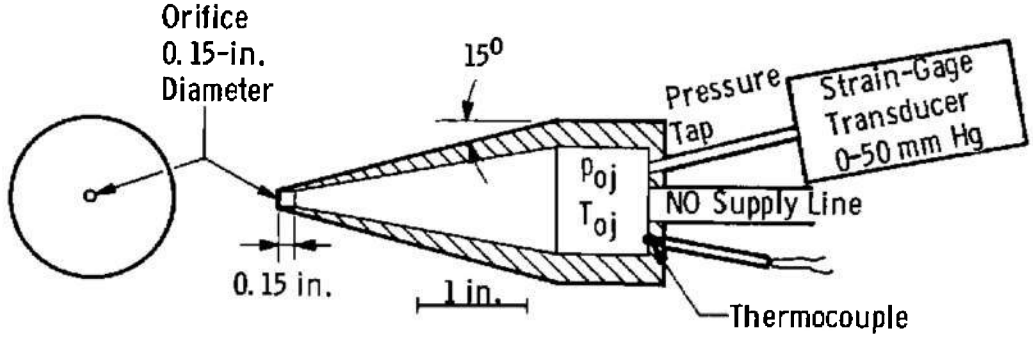

b. Model 2

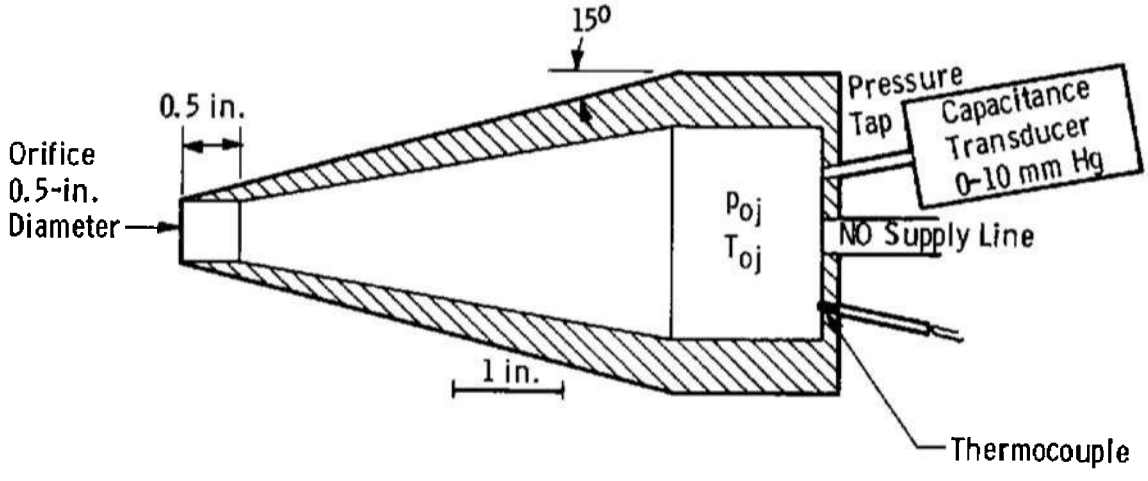

c. Model 3

Fig. 6 Models 1, 2, and 3

Nitric oxide was supplied to the models from standard gas bottles, necessary valving, and flowmeters outside the chamber. To prevent the model gas supply line from being cooled by radiation to the cold chamber walls, heaters on the line maintained the temperature at 290°K.

5.4 FLOW VISUALIZATION

Radio-frequency (R-F) excitation (N_2 afterglow) was used to visualize the gross structure (i.e., shocks) of the flow field. Two R-F generators were used. The R-F signal produced by the two generators caused the flow field to be illuminated, and the outer shock could be clearly distinguished for most of the flow conditions. One antenna was attached to the insulated copper ring at the nozzle exit plane. The other antenna was attached to the model, which was insulated from its supports by a nylon insert (Fig. 7). The chamber was the ground for both generators.

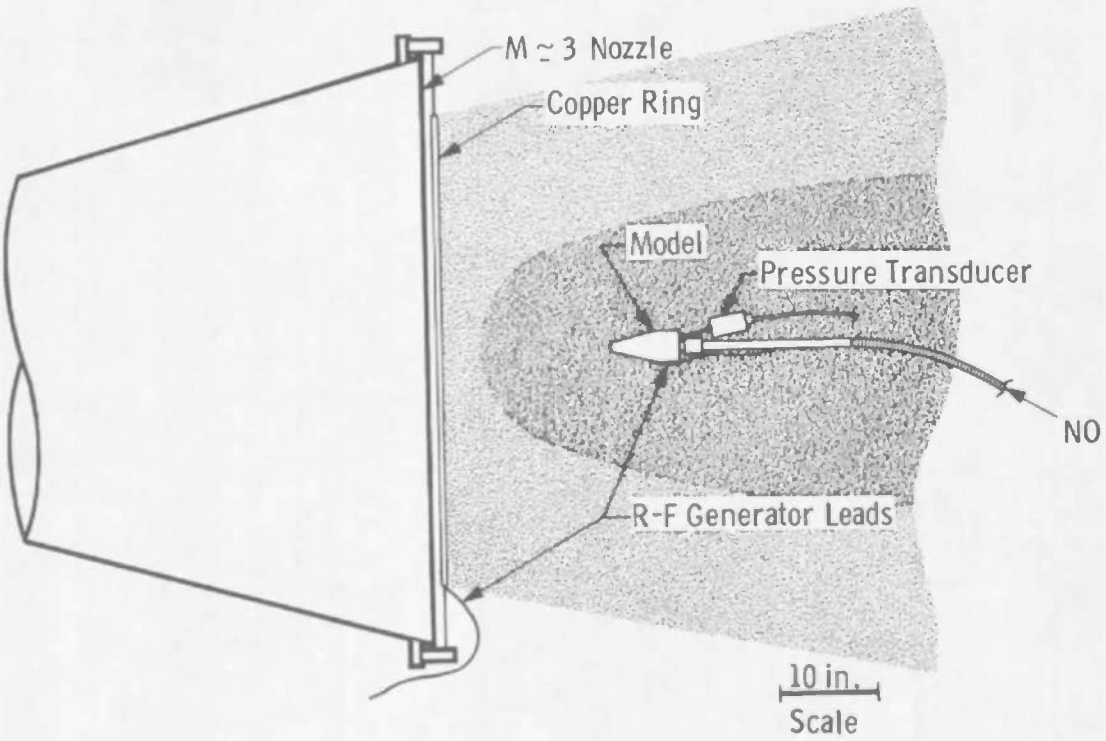

Fig. 7 Model Installation and Flow Visualization

5.5 PHOTOGRAPHIC TECHNIQUE AND ANALYSIS

Photographs of the model and illuminated flow field were made through a chamber port with a 35-mm camera with a f/1.8 lens using black and white Kodak® Plus-X film. Figure 8 shows a typical photograph of the flow

configuration. Microdensitometer traces of the film negatives (for example, Fig. 9) were made to determine the relative positions of the shock and the orifice exit along the centerline of the model. The model diameter was used as a reference dimension on the negatives. A definite shock position was difficult for the $T_{O\infty}$ = 700°K runs because of the gradual film negative density change caused by the thick shocks at these low densities.

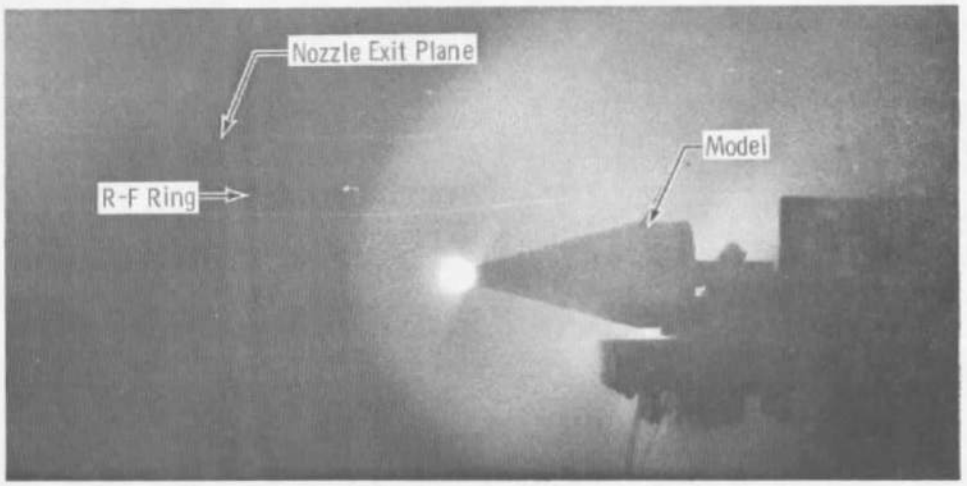

Fig. 8 Typical Photograph of Illuminated Flow Field

Fig. 9 Microdensitometer Trace

SECTION VI
RESULTS AND DISCUSSION

6.1 EXPERIMENTAL RESULTS

The location of the outer shock relative to the orifice position is nondimensionalized by the respective orifice diameter and is plotted versus $P_{0j}/P'_{0\infty}$ in Fig. 10 for all the runs. Since the Mach number range (M_∞) in the tests was relatively low, all the data have been plotted together so that the overall trend in the data can be seen. Equations (4), (40), and (42) are also indicated along with the predicted outer shock location using Fig. 4 for the Mach number range in the experiments. The results show $(R_e/D)_{exp} > (R_e/D)_{theo}$ by 10 to 20 percent for all conditions tested.

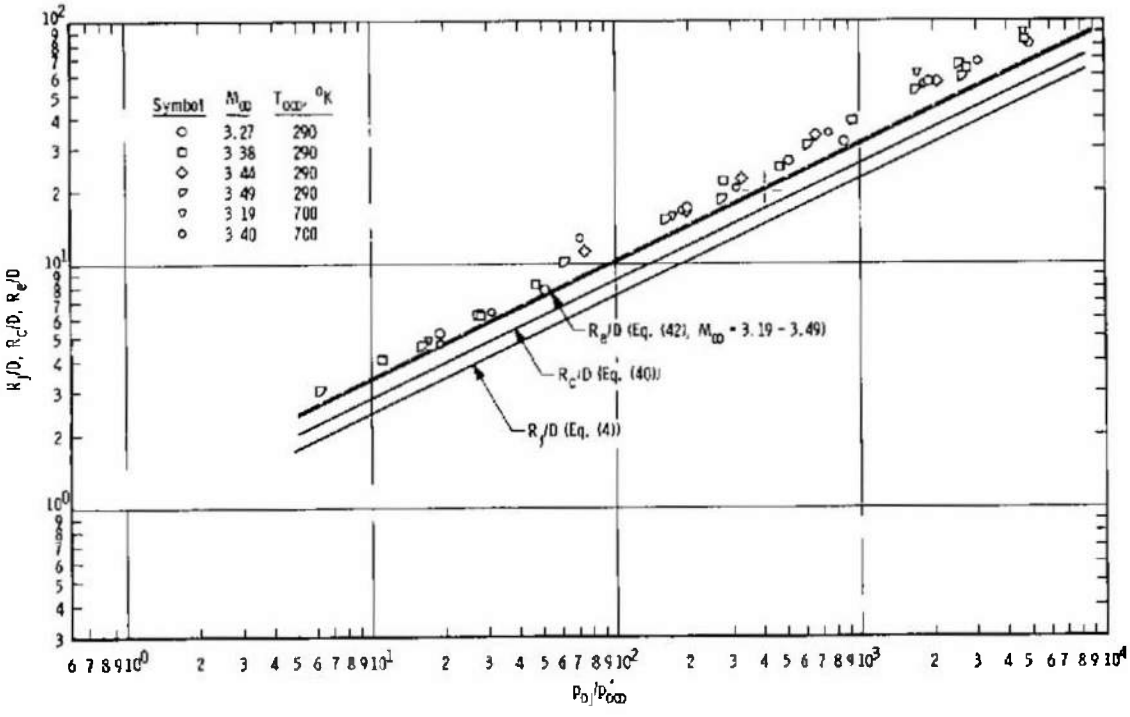

Fig. 10 Experimental Outer Shock Positions

Neither the contact surface nor the inner shock could be seen during the runs or on the photographs. Since a thorough investigation of the excitation and emission mechanisms of the glow is beyond the scope of this report, it can only be suggested that flow inside the free-jet boundary shock was not excited sufficiently to produce a distinct glow intensity change at the inner shock position.

Since neither the contact surface nor the inner shock could be seen, it is difficult to ascertain a priori if the discrepancy is caused by error in the theoretical prediction or by rarefaction effects on the flow field. Note that R_j/D from Eq. (4) is approximately 5 percent less than previous experimental data in Fig. 3, which could account for some of the discrepancy here. By examining other works (Refs. 11, 12, and 13) on low density gas dynamic effects, the present data trend can be seen to be logical for the Reynolds number range of the experiment.

6.2 FLOW RAREFACTION EFFECTS

For the case where the molecular mean free path is small in comparison to a characteristic dimension, the gas may be considered a continuum, and gross changes in the flow field (i.e., shock waves) occur over a very short distance. However, if the mean free path is of the same order-of-magnitude as the characteristic dimension, gross changes in the flow field may occur over distances comparable to the characteristic dimension. The rarefied flow field investigated herein differs from the idealized inviscid case considered in Section IV in that the inner and outer shocks can no longer be considered discontinuities, and the shock thicknesses become significant in comparison with the total shock-layer thickness.

Again considering the similarity of the present flow field and a blunt-body flow field, it can be shown that the effects of flow rarefaction in the present flow field would be similar to low density effects in blunt-body flow. The viscous shock layer on blunt bodies in rarefied flow has been discussed in Refs. 11 and 12. As the Reynolds number, based on sphere radius and viscosity downstream of the normal shock, decreases below ≈1000, the stagnation point shock detachment distance at first decreased slightly and then increased rapidly below Re ≈ 1000. Bailey and Sims (Ref. 13) confirmed this trend for spheres and flat-faced bodies in low density, hypersonic, argon (Ar) flow. These trends in the shock detachment distance for spheres in the transition regime can be applied to the flow field considered here if the boundary conditions are similar for both cases.

Note that the boundary conditions for the viscous shock-layer stagnation point solution are basically the same as the boundary conditions for the present flow field; i.e., the normal velocity component at the contact surface (wall) ≈ 0, and the conditions behind the shock are given by the Rankine-Hugoniot relations or a Navier-Stokes analysis. The Rankine-Hugoniot relations give the conditions behind the normal shock for the thin shock case. For the thick shock case, the flow field from the free stream (or jet flow) to the contact surface must be completely coupled with

a system of equations such as the Navier-Stokes equations (Ref. 12). Figure 11 shows the low density flow field.

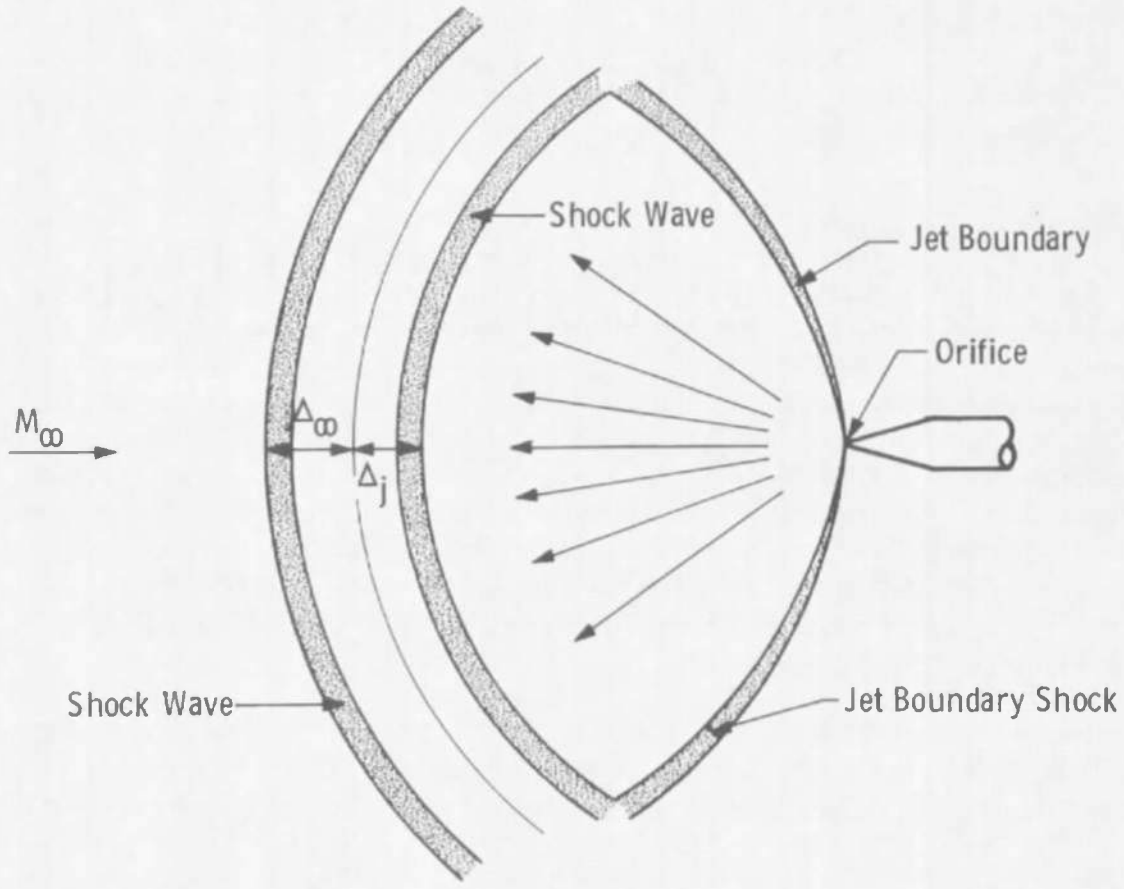

Fig. 11 Sonic Jet Exhausting Counter to a Low Density Supersonic Airstream

Table II shows the Reynolds numbers for the jet and free-stream flow fields based on the calculated inviscid shock detachment distance (Eq. (42) and Fig. 4) and viscosity behind the normal shock,

$$Re_{\infty\Delta_\infty} = \frac{\rho_\infty U_\infty \Delta_\infty}{\mu_{o_\infty}}$$

and

$$Re_{j\Delta_j} = \frac{\rho_j U_j \Delta_j}{\mu_{oj}}$$

Remembering that for hypersonic flow (Ref. 14),

$$\frac{\Delta}{R_{equiv}} \approx \epsilon$$

then

$$Re_{\infty\Delta_\infty} = \frac{\rho_\infty U_\infty R_{equiv}\epsilon}{\mu_{o\infty}} \approx Re_{R_{equiv}}\,\epsilon \qquad (43)$$

and

$$Re_{j\Delta_j} \approx \frac{\rho_j U_j R_{equiv}}{\mu_{oj}} \epsilon \approx Re_{R_{equiv}} \epsilon \tag{44}$$

the low Reynolds number effects on the blunt-body shock detachment distance can be applied. Therefore, low Reynolds number effects would be possible in the present case for

$$Re_{\infty\Delta_\infty} = Re_{j\Delta_j} < 170, \gamma = 1.4 \tag{45}$$

with rapid increases in Δ for

$$Re_{\infty\Delta_\infty} = Re_{j\Delta_j} < 17, \gamma = 1.4 \tag{46}$$

The Reynolds numbers listed in Table II are then in the range where increases in the shock detachment distances would be expected. Rarefaction of the jet and/or the free-stream flow would cause the observed increase in R_e/D. Normally, one would expect rarefaction of both flow fields simultaneously unless gases of widely differing properties are used.

TABLE II
MODEL CONDITIONS AND FLOW REYNOLDS NUMBERS

Model	P_{oj}, mm Hg	T_{oj}, °K	Re_{D*}	$Re_{j\Delta_j}$	$Re_{\infty\Delta_\infty}$
1	44 to 223	290	1100 to 5580	40.8 to 74.2	1.113 to 10.58
2	5 to 22	290	375 to 1650	33.1 to 40.3	1.14 to 10.40
3	0.5 to 2.2	290	125 to 550	34.2 to 39.2	1.19 to 11.58

The assumption of a distinct contact surface, as was done for the inviscid solution, would not be valid as the density in the shock layer is reduced. Considering the flow in the shock layer on a microscopic scale, the migration of one species of gas across the "contact surface" would increase as the density is reduced and mean free path increases. As both shocks become very thick, the shock layer would become fully merged. The analysis would then necessarily be completely coupled to determine species concentration profiles in the shock layer.

Viscous effects at the orifice should also be mentioned. The Reynolds number ranges, based on sonic conditions and the orifice diameter ($Re_{D*} = \rho^* U^* D^*/\mu^*$), are shown in Table II. Results by Ashkenas and Sherman (Ref. 7) and Smetana, et al. (Ref. 15) for a similar type of nozzle indicated viscous influences on the "effective" orifice diameter to be present for $Re_{D*} < 600$. Based on this estimate, viscous influences

on the effective orifice diameter would be expected for Models 2 and 3. If an effective orifice diameter has been used in Eqs. (4), (40), and (42) and for nondimensionalizing the experimental data, both the theoretical lines and the data points would be shifted equally, and the trend would remain.

SECTION VII
CONCLUDING REMARKS

A method for calculating the inviscid flow field structure of a sonic jet exhausting counter to a supersonic airstream has been developed along the centerline. The predicted inner shock to orifice exit distance shows good agreement with previously published data in the continuum flow regime. The data reported herein which were obtained in the transition flow regime indicate that the outer shock to orifice exit distance is greater than the predicted inviscid value. The trend appears to be correct for this flow regime.

Several recommendations for future study can be made based on the present experiment:

1. Extend the test regime to lower and higher densities so that continuum regime data can be obtained to better confirm the theory and low transition regime data can better define the trend with decreasing Reynolds numbers.
2. Develop techniques to locate the inner shock position for all flow regimes, possibly using an electron beam.
3. Investigate the effects of mixing at the contact surface using gases with widely differing thermodynamic properties.

REFERENCES

1. Watts, G. A. "An Experimental Investigation of a Sonic Jet Directed Upstream against a Uniform Supersonic Flow." University of Toronto Institute of Aerophysics Technical Note No. 7, Toronto, Ontario, January 1956.
2. Romeo, D. J. and Sterrett, J. R. "Exploratory Investigation of the Effect of a Forward-Facing Jet on the Bow Shock of a Blunt Body in a Mach Number 6 Free Stream." NASA TN-D-1605, Langley Research Center, Hampton, Virginia, February 1963.

3. Charwat, Andrew F. "Investigation of the Flow and Drag due to Supersonic Jets Discharging Upstream into a Supersonic Flow." Rand-P-2943, The Rand Corporation, Santa Monica, California, July 1964.

4. van der Bliek, J. A. and Cassanova, R. A. "Simulation of Chemiluminescent Reaction of Nitric Oxide with Atomic Oxygen in a Supersonic Low Density Wind Tunnel - Interim Report." AEDC-TR-66-105 (AD636982), August 1966.

5. Good, R. E. and Hill, J. A. F. "A Wind Tunnel Investigation of the Nitric Oxide-Oxygen Reaction." MC64-116-R1, Mithras, Inc., Cambridge, Massachusetts, March 1966.

6. van der Bliek, J. A. and Cassanova, R. A. "Simulation of Chemiluminescent Reaction of Nitric Oxide with Atomic Oxygen in a Supersonic Low Density Wind Tunnel - Part 2." AEDC-TR-66-254 (AD645516), January 1967.

7. Ashkenas, Harry and Sherman, F. S. "The Structure and Utilization of Supersonic Free Jets in Low Density Wind Tunnels." Rarefied Gas Dynamics, Vol. 2, Academic Press, 1966, pp. 84-105.

8. Sherman, F. S. "Self-Similar Development of Inviscid Hypersonic Free-Jet Flows." Lockheed Missiles and Space Company Report 6-90-63-61, Sunnyvale, California, May 1963.

9. Li, Ting-Yi, and Geiger, Richard E. "Stagnation Point of a Blunt Body in Hypersonic Flow." Journal of the Aeronautical Sciences, Vol. 24, No. 1, January 1957, pp. 25-32.

10. van Dyke, M. D. "A Model of Supersonic Flow Past Blunt Axisymmetric Bodies, with Application to Chester's Solution." Journal of Fluid Mechanics, Vol. 3, pp. 515-522, 1958.

11. Ho, Hung-Ta, and Probstein, Ronald F. "The Compressible Viscous Layer in Rarefied Hypersonic Flow." ARL-TN-60-132 (AD243764), Brown University, Providence, Rhode Island, August 1960.

12. Goldberg, L. "The Structure of the Viscous Hypersonic Shock Layer." General Electric R-658-D50, Missile and Space Division, Philadelphia, Pennsylvania, December 1965.

13. Bailey, A. B. and Sims, W. H. "The Shock Shape and Shock Detachment Distance for Spheres and Flat-Faced Bodies in Low-Density, Hypervelocity, Argon Flow." AEDC-TDR-63-21 (AD297197), February 1963.

14. Probstein, Ronald F. and Kemp, Nelson H. "Viscous Aerodynamic Characteristics in Hypersonic Rarefied Gas Flow." Journal of the Aerospace Sciences, Vol. 27, March 1960, pp. 174-192.

15. Smetana, F. O., Sherrill, W. A., II, and Schort, D. R., Jr. "Measurements of the Discharge Characteristics of Sharp-Edged and Round-Edged Orifices in the Transition Regime." Rarefied Gas Dynamics, Vol. 2, Academic Press, 1967, pp. 1243-1256.

UNCLASSIFIED
Security Classification

DOCUMENT CONTROL DATA - R & D

(Security classification of title, body of abstract and indexing annotation must be entered when the overall report is classified)

1. ORIGINATING ACTIVITY (Corporate author)	2a. REPORT SECURITY CLASSIFICATION
Arnold Engineering Development Center, ARO, Inc., Operating Contractor, Arnold Air Force Station, Tennessee	UNCLASSIFIED
	2b. GROUP N/A

3. REPORT TITLE

FLOW FIELD OF A SONIC JET EXHAUSTING COUNTER TO A LOW DENSITY SUPERSONIC AIRSTREAM

4. DESCRIPTIVE NOTES (Type of report and inclusive dates)

April 25-29, 1966 Final

5. AUTHOR(S) (First name, middle initial, last name)

Robert A. Cassanova, ARO, Inc.

6. REPORT DATE	7a. TOTAL NO. OF PAGES	7b. NO OF REFS
October 1967	31	15

8a. CONTRACT OR GRANT NO	9a. ORIGINATOR'S REPORT NUMBER(S)
AF40(600)-1200 b. Program Element 62405424 c. 7635 d.	AEDC-TR-67-149
	9b. OTHER REPORT NO(S) (Any other numbers that may be assigned this report) N/A

10 DISTRIBUTION STATEMENT This document has been approved for public release and sale; its distribution is unlimited.

11. SUPPLEMENTARY NOTES	12 SPONSORING MILITARY ACTIVITY
Available in DDC.	AF Cambridge Research Laboratory (CRUI), Air Force Systems Command, Hanscom Field, Bedford, Mass.

13 ABSTRACT

The flow field of a sonic jet exhausting counter to a supersonic airstream has been investigated theoretically and experimentally. The total shock-layer thickness was calculated using a blunt-body-type analysis and the known properties of a free-jet expansion from a sonic orifice. The total shock-layer thickness and position of the outer shock relative to the orifice are shown to be a function of free-stream Mach number, jet reservoir pressure, free-stream pitot pressure, and orifice size. The predicted inner shock position is compared with previously published experimental data, and the predicted outer shock position is compared with data obtained in a low density wind tunnel. Results in the transitional flow regime indicate that the outer shock to orifice position distance is greater than the predicted value.

DD FORM 1 NOV 65 1473

UNCLASSIFIED
Security Classification

14 KEY WORDS	LINK A		LINK B		LINK C	
	ROLE	WT	ROLE	WT	ROLE	WT
sonic jets						
flow fields						
blunt bodies						
shock-layer thickness						
supersonic flow						
counter exhaust						